

# Hybrid fiber links for accurate optical frequency comparison

Won-Kyu Lee<sup>1,3,4</sup> · Fabio Stefani<sup>1,2</sup> · Anthony Bercy<sup>2,1</sup> · Olivier Lopez<sup>2</sup> · Anne Amy-Klein<sup>2</sup> · Paul-Eric Pottie<sup>1</sup> 

Received: 26 January 2017 / Accepted: 19 April 2017 / Published online: 2 May 2017  
© The Author(s) 2017. This article is an open access publication

**Abstract** We present the experimental demonstration of a local two-way optical frequency comparison over a 43-km-long urban fiber network without any requirement for measurement synchronization. We combined the local two-way scheme with a regular active noise compensation scheme that was implemented on another parallel fiber leading to a highly reliable and robust frequency transfer. This hybrid scheme allowed us to investigate the major limiting factors of the local two-way comparison. We analyzed the contributions of the interferometers at both local and remote locations to the phase noise of the local two-way signal. Using the ability of this setup to be injected by either a single laser or two independent lasers, we measured the contributions of the demodulated laser instabilities to the long-term instability. We show that a fractional frequency instability level of  $10^{-20}$  at 10,000 s can be obtained using this simple setup after propagation over a distance of 43 km in an urban area.

## 1 Introduction

The technique of phase-compensated optical fiber link [1–5] has developed rapidly over the last decade and has enabled the transfer and comparison of optical frequencies over continental-scale distances of more than 1000 km [6–9]. Optical fiber-based clock frequency comparison is not only useful for time–frequency metrology, but can also provide a powerful experimental tool in many applications, such as test of variation of fundamental constants [10], relativistic geodesy [6], and dark matter search [11].

Optical frequency transfer by the active noise cancellation (ANC) method [1, 12] has a wide range of applications, including remote high-resolution and high-accuracy spectroscopy [13–15], very long baseline interferometry [16], and remote narrow-linewidth light sources [2, 14, 17]. However, if only a comparison of the optical frequencies is required, the recently proposed two-way method [18–20] offers a good alternative with the advantage of simplified experimental apparatus without active components. In this method, the fiber noise is eliminated from the frequency comparison signal by post-processing of the data that were obtained synchronously at both sites in the same way as in the two-way satellite time and frequency transfer technique [21].

The optical two-way time and frequency transfer technique was introduced in [22] over a 2-km-long free space link via two-way exchange between frequency combs using time-of-flight measurements. The two-way optical phase comparison technique using a fiber network was first introduced in [18], in which a Sagnac interferometer configuration was used to compare ultra-stable lasers through a 47-km-long fiber link. This method was further investigated in [19, 20] via a novel local two-way (LTW) comparison scheme, in which the fiber noise can be suppressed

---

✉ Paul-Eric Pottie  
paul-eric.pottie@obspm.fr

<sup>1</sup> Laboratoire National de Métrologie et d’Essais–Système de Références Temps-Espace (LNE-SYRTE), Observatoire de Paris, CNRS, UPMC, Paris, France

<sup>2</sup> Laboratoire de Physique des Lasers, Université Paris 13, CNRS, Villetaneuse, France

<sup>3</sup> Korea Research Institute of Standards and Science, Daejeon 34113, South Korea

<sup>4</sup> University of Science and Technology, Yuseong, Daejeon 34113, South Korea

in real time, by using measurements from one link end only that were performed at either the local site or the remote site. After the method was initially introduced with a uni-directional configuration that used a pair of parallel fibers over an urban network [19], it was subsequently presented using a fully bi-directional configuration over a 25-km-long fiber spool [20]. The LTW method has several advantages when compared with the conventional two-way (CTW) method. First, because only local measurement data are used, there is no need for synchronization of the measurements between the local site and the remote site to remove the fiber noise, and real-time frequency comparison is thus possible. Second, the results of the two LTW measurements (one performed at the local site and the other at the remote site) can be compared and cross-checked in post-processing, and a CTW observable can then be formed. This method allows us to perform several self-consistency checks on the signals that are provided by redundant detection, which enable the diagnosis of cycle-slips and the discrimination of their origin. Note that the results that were reported in [18–20] were from proof-of-principle experiments in which both fiber ends were located at the same laboratory (i.e., the local site and the remote site were the same place), and the two laser sources to be compared were actually the same laser.

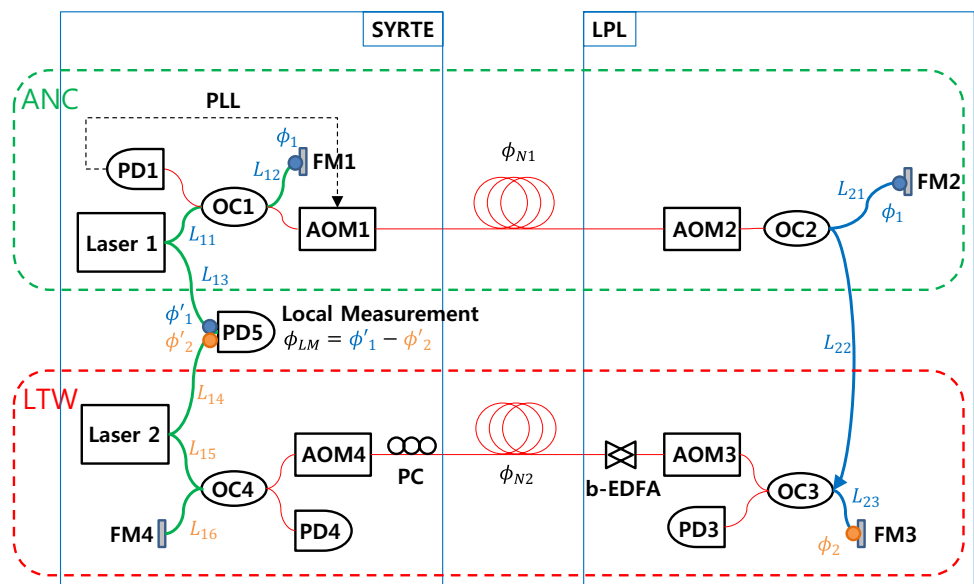
In this report, we present our experimental work on a  $2 \times 43$  km fiber link that connects SYRTE (Système de Références Temps-Espace) to LPL (Laboratoire de Physique des Lasers) through a dedicated fiber pair over an urban area. In the perspective of the forthcoming optical clock comparison that is to be accomplished between the National Physical Laboratory (NPL) in the UK and SYRTE in France, we were seeking a robust scheme with ultimate

stability and accuracy [23, 24]. With that purpose, we investigated a hybrid architecture that uses active compensation on one of the fibers and uses a local two-way setup on the other fiber [25]. We report here, to the best of our knowledge, the first experimental results of optical frequency comparison using the LTW scheme on an installed fiber network and in a realistic implementation. We investigate the effects of ultra-stable laser instability on the fiber link noise floor using two independent laser sources for the LTW comparison. The limiting factors of the frequency comparison capability of the LTW scheme have been investigated rigorously, and their contributions to the relative frequency instabilities are presented and discussed. Finally, we discuss the accuracy of the frequency transfer and show that the hybrid setup allows optical clock comparison to the  $10^{-20}$  level.

## 2 Schematic overview of experimental methods for optical frequency comparison

The experimental scheme that we implemented for optical frequency transfer and comparison is shown in Fig. 1. The experiments were performed using a pair of 43-km-long dedicated fibers on an urban network [3, 26, 27] that links SYRTE and LPL, which are two laboratories located in the urban area of Paris. The two fibers are denoted by fiber-1 and fiber-2. On fiber-1, we built a regular setup that used active noise compensation (ANC) of the fiber noise. On fiber-2, we built the local two-way setup that was introduced in [20]. We used two independent ultra-stable lasers that operated at  $1.5 \mu\text{m}$ , with sub-Hz linewidths, and typical frequency drifts of approximately 1 Hz/s.

**Fig. 1** Experimental scheme for simultaneous optical frequency transfer and comparison. *PD* photodiode, *FM* Faraday mirror, *OC* optical coupler, *AOM* acousto-optic modulator, *PLL* phase-locked loop, *b-EDFA* bi-directional erbium-doped fiber amplifier, *PC* polarization controller. The upper part in the *green dashed box* shows the ANC setup on fiber-1, and the lower part in the *red dashed box* shows the LTW setup on fiber-2. *L<sub>s</sub>* represent the lengths of the fiber segments (which are shown with *thick lines*), and  $\phi_s$  represent the optical phase of the laser beams at the *filled circles*



For the ANC setup, we used a fiber interferometric setup. The light from Laser1 was split into two branches, and optical couplers were used to implement Michelson-like interferometers. The interferometric setup at SYRTE was realized using spliced components and was placed in an aluminum box that was surrounded with thick thermal insulating foam. At the coupler output, we set up a fiber-pigtailed acousto-optic modulator (AOM1) to provide feedback for noise compensation. The light was then injected into the long-haul dedicated fiber that connects the two laboratories. The light at the remote end was frequency-shifted by AOM2 (which provided a constant shift) to distinguish the signal from spurious reflections, and part of this light was reflected back by a Faraday mirror (FM2). The fiber noise ( $\phi_{NI}$ ) was measured after a round trip using a photodiode (PD1) to detect the beat note between the round-trip signal and the light that was reflected by another Faraday mirror (FM1) at SYRTE. The beat signal was tracked and processed to provide active compensation of the fiber noise by acting on the carrier frequency of AOM1. The local optical phase ( $\phi_l$ ) at FM1 is copied to the remote Faraday mirror (FM2) using this ANC setup, as described in the Appendix. These two points are shown in Fig. 1 as blue filled circles. For the local interferometric setup at SYRTE, the sensitivity of the differential optical phase to temperature, as defined in [20], was measured to be 7 fs/K. The frequency transfer performance on this link was reported previously in [3, 26, 27].

To check the relative frequency stability and accuracy of the ANC setup, we cascaded the two 43-km fibers to form an 86-km-long fiber loop as described in [3, 26, 27]. The frequency of the beat-note signal between the local laser beam and the beam transmitted at the output of the 86-km long fiber was measured simultaneously using two dead-time-free counters [28] (where one was  $\Pi$ -type and the other was  $\Lambda$ -type [29, 30]) with a gate time of 1 s. No cycle slip was observed in the frequency data throughout the total measurement time of 66 691 s. The fractional frequency instabilities of the ANC transfer method in terms of the Allan deviation [29, 30] are shown in Fig. 2. The uncompensated 86 km fiber noise is also shown as a light gray solid line. The overlapping Allan deviation (ADEV) and the modified Allan deviation (MDEV) that were calculated from the  $\Pi$ -type counter data started from  $1.4 \times 10^{-15}$  at 1 s and decreased with slopes of  $-1$  and  $-3/2$ , respectively, which is as expected for white phase noise. The ADEV and the MDEV that were calculated from the  $\Lambda$ -type counter data started from  $2.4 \times 10^{-17}$  at 1 s and decreased to  $1 \times 10^{-20}$  and to  $6 \times 10^{-21}$  at 10,000 s, respectively. The MDEVs of the data that were recorded using the  $\Pi$ -type and  $\Lambda$ -type counters converged to the same value and showed good agreement. This limit is attributed to the phase variation that is related to the temperature

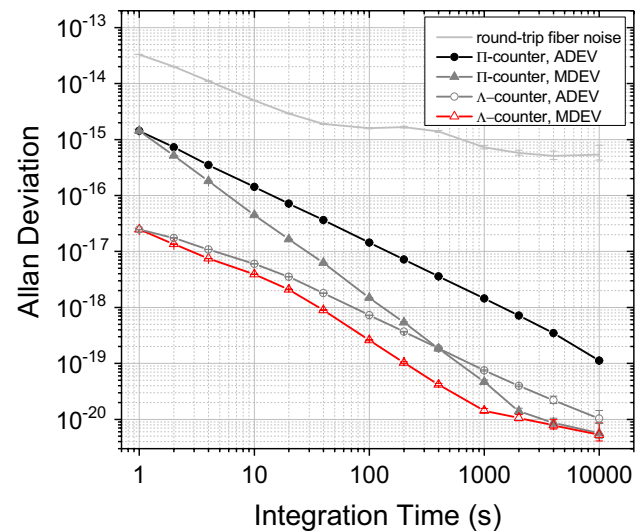


**Fig. 2** Fractional frequency instabilities of active noise compensation in terms of the Allan deviation with a  $\Pi$ -type counter and a  $\Lambda$ -type counter in an end-to-end (86 km) scheme. ADEV the overlapping Allan deviation, MDEV the modified Allan deviation

fluctuations of the residual fiber-length mismatch in the interferometer [20]. The mean frequency offset from the expected frequency of the remote output was calculated using the total  $\Lambda$ -type counter data to be  $8 \times 10^{-21}$  with a statistical uncertainty of  $1 \times 10^{-20}$  (based on the long-term overlapping ADEV at 10,000 s with  $\Lambda$ -data [31–33]). This result is consistent with the mean frequency offset of  $1.2 \times 10^{-20}$  of the total  $\Pi$ -type counter data and its statistical error of  $1.7 \times 10^{-20}$  (which was calculated as the relative standard deviation divided by the number of consecutive data in this white phase noise case [19, 34]). This shows the reliability of this uncertainty value. Therefore, it can be concluded that the optical phase of the local laser has been transferred to the 86-km-long link output end with an accuracy of  $<2 \times 10^{-20}$  using the ANC method and that no frequency bias was observed within the statistical uncertainty of the data set.

We used the ANC setup (which is shown in the green dashed box in Fig. 1) to transfer the phase of Laser1 to the remote site, and used the transferred Laser1 beam as a remote laser that is to be compared with a second laser (Laser2) at local site by the LTW method. In the hybrid frequency comparison setup shown in Fig. 1, part of the light that reached the remote site was extracted and was then re-injected into the second fiber that connects the two laboratories. This second part of the setup is depicted in the lower part of Fig. 1. The LTW experimental setup only is shown and explained in Fig. 7 in the “Appendix”. On each side, an optical coupler was used to realize a strongly unbalanced Michelson interferometer and an AOM was used to apply a constant frequency shift to the laser light. A polarization

controller and Faraday mirrors were used so that the beat-note signals on PD3 and PD4 were optimized. A bi-directional erbium-doped fiber amplifier (b-EDFA) was used at the remote site to compensate for the transmission loss of Laser1. As described in the Appendix and in [20], two signals were generated in each photodiode: one was the signal for the frequency difference between the local laser and the laser that was transmitted from the remote site, and the other was the signal for the fiber noise measurement. The fiber noise  $\phi_{N2}$  could be measured at the local PD4 using the round-trip signal of the local laser, if  $\phi_{N2}$  was assumed to be the same in both uplink and downlink transmission. Alternatively,  $\phi_{N2}$  could also be measured at the remote PD3 using the round-trip signal of the remote laser in a similar way. A more detailed description of the signal processing is given in the next section.

The real local measurement (LM) of the frequency difference between the two lasers was performed using a photodiode (PD5) at the local site for the comparison with the LTW measurement results.

When the CTW method is used, the fiber noise  $\phi_{N2}$  is not measured but is eliminated from the frequency difference signal using a combination of the two beat-note signals that are recorded at each of the end sites on both local PD4 and remote PD3. Because  $\phi_{N2}$  is assumed to be the same in the two signals from PD3 and PD4, it can then be eliminated by post-processing the two measurement data sets. The local data and the remote data should be measured synchronously [18]. Unlike the CTW method, the LTW method uses only the local measurement data, and thus there is no need for data exchange between the local and remote sites for post-processing or for synchronization of the data acquisition timing. However, the noise rejection can be up to four times lower in the power spectral density in the LTW method because it is limited by the propagation time, which is twice as long for the round-trip signal when compared with that for the CTW method [20]. In addition, the LTW method is more sensitive to fiber attenuation because it requires round-trip propagation in the same fiber, whereas the CTW method only requires one-way propagation.

To compare independent laser sources at the remote site, we used one of the fibers to transfer the ultra-stable laser light from SYRTE to LPL using the ANC setup as shown in Fig. 1, and we used the LTW setup to inject a second independent ultra-stable laser in the second fiber. In this way, we used the second fiber to perform the LTW comparison between two independent ultra-stable lasers. We also performed a second series of experiments using only one ultra-stable laser. In that case, the instabilities arising from the ultra-stable laser frequency fluctuations were largely rejected, and the interferometric noise could thus be

studied with deeper insights. All frequencies were recorded using dead-time-free frequency counters [28].

Note that this hybrid configuration not only allows us to study the performance of the LTW scheme, but also offers a very convenient way to transfer an ultra-stable laser signal to the remote site with real-time evaluation of both the transfer accuracy and the stability thanks to the LTW signal at the remote site. Moreover, this performance can be checked further using the LTW signal at the local site and the CTW method, thus demonstrating that this hybrid fiber link design provides a highly reliable frequency transfer technique.

### 3 Local two-way experiments

The LTW measurement at the local site was performed using the two signals on PD4:  $\phi_{PD4A} = (\phi_{L1} + \phi_{N2}) - \phi_{L2}$  is a measure of the fiber noise-uncompensated phase difference between the two laser beams (with respective phases given by  $\phi_{L1}$  and  $\phi_{L2}$ ), and  $\phi_{PD4B} = 2\phi_{N2}$  is a measure of the round-trip fiber noise (see the ‘‘Appendix’’). We used a heterodyne detection technique to generate all the signals on a single photodiode. We engineered the frequency map to ensure that the signals were sufficiently far apart to be filtered and separated easily. Each filtered signal was amplified and tracked using a tracking oscillator with a typical bandwidth of 100 kHz. The compensated LTW phase difference,  $\phi_{LTW}^{local}$ , that was measured at the local site is given by [20]

$$\phi_{LTW}^{local} = \phi_{PD4A} - \frac{\phi_{PD4B}}{2} = \phi_{L1} - \phi_{L2}. \quad (1)$$

It should be noted that  $\phi_{LTW}^{local}$  is measured only using the local measurements taken by PD4.

Similarly, the LTW measurement is also possible at the remote site by using the two corresponding signals on PD3, which are given by  $\phi_{PD3A} = (\phi_{L2} + \phi_{N2}) - \phi_{L1}$  and  $\phi_{PD3B} = 2\phi_{N2}$ . The compensated LTW phase difference that was measured at the remote site,  $\phi_{LTW}^{remote}$ , is given by

$$\phi_{LTW}^{remote} = \phi_{PD3A} - \frac{\phi_{PD3B}}{2} = \phi_{L2} - \phi_{L1}. \quad (2)$$

Meanwhile, a CTW measurement is also possible using this setup. The compensated CTW phase difference  $\phi_{CTW}$  is given by

$$\phi_{CTW} = \frac{\phi_{PD4A} - \phi_{PD3A}}{2} = \phi_{L1} - \phi_{L2} \quad (3)$$

In Eq. 3, it should be noted that measurement of  $\phi_{CTW}$  requires that the data sets that are measured at both the local and remote sites be synchronized [18].

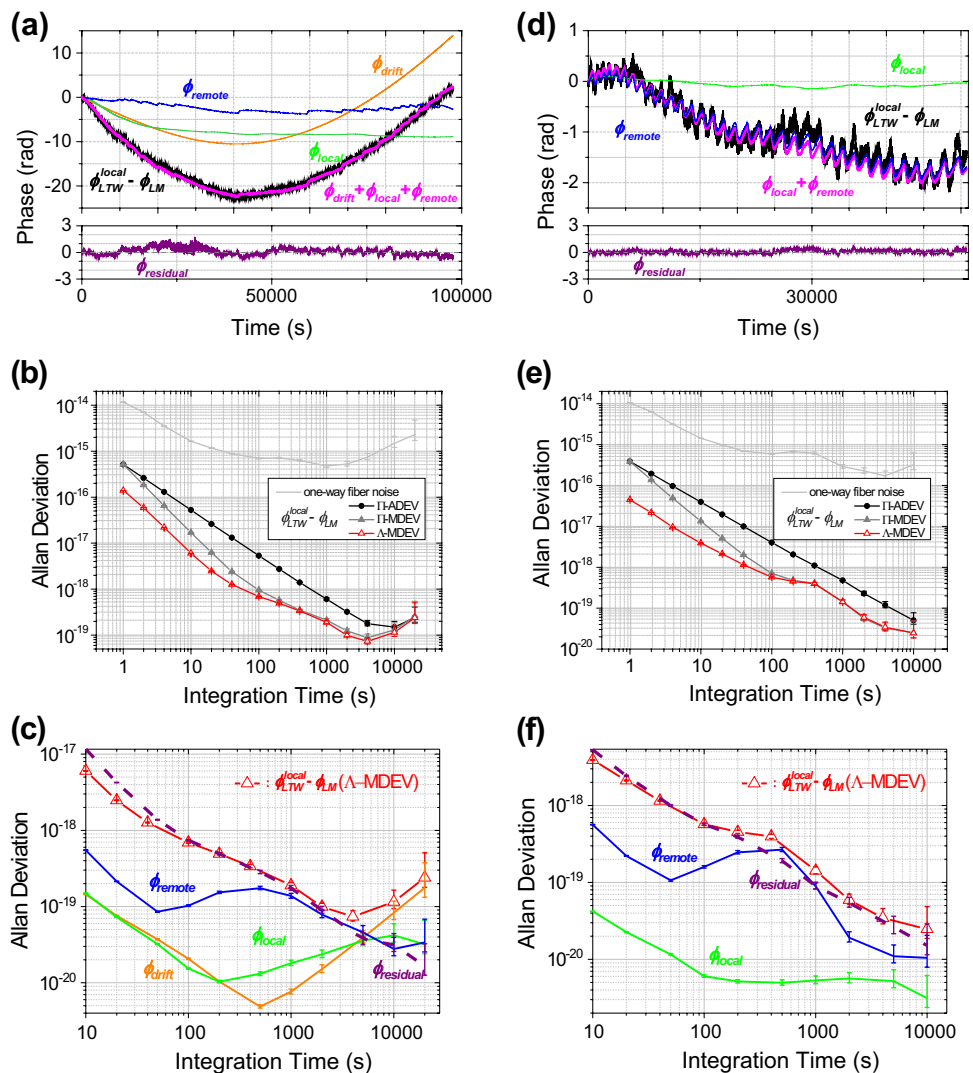
To test the performance of the LTW method, the result of the  $\phi_{LTW}^{local}$  measurement was compared with the real local measurement  $\phi_{LM}$  using the frequency data that were obtained simultaneously using a  $\Pi$ -type counter and a  $\Lambda$ -type counter with a gate time of 1 s. The real local measurement is given by  $\phi_{LM} = \phi'_1 - \phi'_2$ , where  $\phi'_1$  ( $\phi'_2$ ) is the phase of Laser1 (Laser2) at PD5. The phase difference  $\phi_{LTW}^{local} - \phi_{LM}$  should be zero in the limit of perfect fiber noise rejection and a perfect experimental setup. The fiber noise rejection is limited by the propagation delay that induces a small difference between the forward and backward propagation noise [12, 20]. Other effects, such as the Sagnac effect or the polarization effects, can also limit the fiber noise rejection performance, which is effective only for fluctuations that are equal for both forward and backward propagation. The measured phase evolution of  $\phi_{LTW}^{local} - \phi_{LM}$  in 100,000 s is shown in Fig. 3a as a thick black line. This phase evolution is attributed to three major sources, which are described in detail below.

When using the ANC setup, it can easily be shown that any linear laser drift will be corrected by the action of the phase-locked loop (PLL) and thus the transferred remote phase directly copies the local phase  $\phi_1$  as if there was no propagation delay (see the Appendix). However, in the LTW case, the drift of the frequency difference between the two laser beams affects the phase of  $\phi_{LTW}^{local} - \phi_{LM}$  because of the time delay  $\tau$  of light propagation between the local site and the remote site. From the derivation shown in the Appendix, the first component of the phase evolution of  $\phi_{LTW}^{local} - \phi_{LM}$  due to the drift of the frequency difference is given by:

$$\phi_{drift} = -2\pi \tau [(v_1(t) - v_2(t)) - (v_1(t_0) - v_2(t_0))], \quad (4)$$

where  $v_1(t)$  and  $v_2(t)$  are the frequencies of Laser1 and Laser2, respectively, at the entrance of the local interferometer at time  $t$ .  $t_0$  is the instant at which the phase measurement started.

**Fig. 3** **a** Phase evolutions of the local two-way comparison and of the three major phase error sources.  $\phi_{LTW}^{local} - \phi_{LM}$  is the phase difference between the local two-way measurement and the real local measurement,  $\phi_{drift}$  is the phase evolution due to the drift of the frequency difference,  $\phi_{local}$  is the phase evolution caused by the length mismatch in the local interferometer,  $\phi_{remote}$  is the phase evolution related to the length mismatch in the remote interferometer, and  $\phi_{residual} = \phi_{LTW}^{local} - \phi_{LM} - \phi_{drift} - \phi_{local} - \phi_{remote}$ . **b** Fractional frequency instability of  $\phi_{LTW}^{local} - \phi_{LM}$  in terms of the Allan deviation, **c** the MDEVs of the three major phase error sources. Independent lasers were used at both sites in cases of **a–c**. Parts **d–f** show results corresponding to each case of **a–c**, respectively, in the case where the same laser was used at both sites



The second component of the phase evolution of  $\phi_{\text{LTW}}^{\text{local}} - \phi_{\text{LM}}$  is caused by the length mismatch  $\delta L_{\text{local}} = (L_{14} + L_{16} - L_{15}) + (L_{11} + L_{12} - L_{13})$  in the local interferometer and is given by

$$\phi_{\text{local}} = 2\pi\nu(\delta L_{\text{local}})\gamma[T_{\text{local}}(t) - T_{\text{local}}(t_0)], \quad (5)$$

where  $\gamma$  is a phase-temperature coefficient of the silica fiber, which has a value of 37 fs/(K·m) for an optical carrier at 194.4 THz and at 298 K [20], and  $T_{\text{local}}(t)$  is the temperature of the local interferometer. This contribution is cancelled out if  $L_{13} = L_{11} + L_{12}$  (which leads to  $\phi'_1 = \phi_1$ ) and  $L_{15} = L_{14} + L_{16}$ . Similarly, the last component of the phase evolution of  $\phi_{\text{LTW}}^{\text{local}} - \phi_{\text{LM}}$  is related to the length mismatch  $\delta L_{\text{remote}} = L_{22} - L_{21} - L_{23}$  in the remote interferometer and is given by

$$\phi_{\text{remote}} = 2\pi\nu(\delta L_{\text{remote}})\gamma[T_{\text{remote}}(t) - T_{\text{remote}}(t_0)], \quad (6)$$

where  $T_{\text{remote}}(t)$  is the temperature of the remote interferometer. This contribution is cancelled out when  $L_{22} = L_{21} + L_{23}$ . In the case of a common laser phase ( $\phi_{L1} = \phi_{L2}$ ), it would result in  $\phi_1 = \phi_2$  where  $\phi_2$  is the phase of Laser2 on FM3 (see Fig. 1).

$\phi_{\text{drift}}$  is shown in Fig. 3a as a thin orange line and was determined using Eq. (4) and the frequency data from the real local measurement on PD5. The temperature data were measured simultaneously at 5 s intervals at both the local interferometer box and the remote interferometer box. A time delay is expected between the measured temperature and the real temperature of the fiber interferometer because of the heat transfer time. These time delays were obtained using a correlation analysis between the phase evolution and the temperature measurements, yielding 2300 s for the local interferometer and 105 s for the remote interferometer. The temperature measurement data were then shifted by these delay times.  $\delta L_{\text{local}}$  and  $\delta L_{\text{remote}}$  were then determined to be 0.15 and 0.35 m, respectively, based on a multi-linear regression of the phase evolution using the local and remote temperature data as the independent variables. As a result,  $\phi_{\text{local}}$  and  $\phi_{\text{remote}}$  are shown in Fig. 3a as a thin green line and a thin blue line, respectively. Figure 3a shows that the phase evolution of  $\phi_{\text{LTW}}^{\text{local}} - \phi_{\text{LM}}$  can be nicely explained as being the sum of the phase errors from these three major components (shown as the thick pink line).

The fractional frequency instabilities in terms of the Allan deviations in Fig. 3b were obtained using these phase evolution data. In Fig. 3c, a magnified view of the MDEV for  $\phi_{\text{LTW}}^{\text{local}} - \phi_{\text{LM}}$  and the instability contributions of the three major phase error sources are also shown;  $\phi_{\text{drift}}$  is indicated by an orange line,  $\phi_{\text{local}}$  is indicated by a green line, and  $\phi_{\text{remote}}$  is indicated by a blue line. The ADEV and the MDEV that were calculated from the  $\Pi$ -type counter data started from  $5 \times 10^{-16}$  at 1 s and decreased with slopes of  $-1$  and  $-3/2$ , respectively, which is as expected

for white phase noise. The MDEV that was calculated from the  $\Lambda$ -type counter data started from  $1.4 \times 10^{-16}$  at 1 s and was limited by the contribution of  $\phi_{\text{remote}}$  from 400 to 2000 s (which was caused by the room temperature control at the remote site), and was then limited by the contribution of  $\phi_{\text{drift}}$  after 10,000 s, resulting in a minimum instability of  $8 \times 10^{-20}$  at 4000 s. The expected frequency instability of the LTW measurement, when the three major phase error components are suppressed, can be calculated using the residual phase, which is given by

$$\phi_{\text{residual}} = \phi_{\text{LTW}}^{\text{local}} - \phi_{\text{LM}} - \phi_{\text{drift}} - \phi_{\text{local}} - \phi_{\text{remote}} \quad (7)$$

This result is shown as a purple dashed line and the ultimate instability would be  $2 \times 10^{-20}$  at 20,000 s with experimental optimization. The ultimate accuracy of the frequency comparison with experimental optimization was then estimated by calculating the mean value of the  $\Lambda$ -type frequency data of  $\phi_{\text{residual}}$ , giving a result of  $6 \times 10^{-21}$  with a statistical uncertainty of  $3 \times 10^{-20}$  (based on the long-term overlapping ADEV at 20,000 s with the  $\Lambda$ -data [31–33]).

Next, we investigated the LTW optical frequency comparison scheme when using the same laser at both sites. This configuration provides an experimental simulation in which the drift of each laser is actively removed.  $\phi_{\text{drift}}$  is zero in this case, and the phase evolution is expected to be governed by the two remaining phase error sources. The measured phase evolution of  $\phi_{\text{LTW}}^{\text{local}} - \phi_{\text{LM}}$  (shown as a thick black line), the estimated phase error due to  $\phi_{\text{local}}$  (shown as a green line), the estimated phase error due to  $\phi_{\text{remote}}$  (shown as a blue line), and the sum of the contributions from the two major phase error sources (shown as a thick pink line) are presented in Fig. 3d. The overall phase evolution of  $\phi_{\text{LTW}}^{\text{local}} - \phi_{\text{LM}}$  is explained by the sum of the two major phase error sources.  $\phi_{\text{residual}}$  is shown in the lower part of Fig. 3d and is well within 1 rad. The fractional frequency instabilities of  $\phi_{\text{LTW}}^{\text{local}} - \phi_{\text{LM}}$  and of the two major phase error sources are shown in Fig. 3e and Fig. 3f, respectively. The ADEV and the MDEV that were calculated from the  $\Pi$ -type counter data started from  $4 \times 10^{-16}$  at 1 s and decreased with slopes of  $-1$  and  $-3/2$ , respectively, which is as expected for white phase noise. The MDEV that was calculated from the  $\Lambda$ -type counter data started from  $5 \times 10^{-17}$  at 1 s and was limited by the contribution of  $\phi_{\text{remote}}$  around 400 s (which was caused by the room temperature control at the remote site), resulting in a minimum instability of  $2.4 \times 10^{-20}$  at 10,000 s. The expected instability of  $\phi_{\text{residual}}$  (represented by a purple dashed line) indicates that the ultimate instability would be  $1.2 \times 10^{-20}$  at 10,000 s if two remaining major error sources were suppressed via fiber-length optimization. The ultimate accuracy of the frequency comparison with experimental optimization was then estimated by calculating the

mean value of the  $\Lambda$ -type frequency data of  $\phi_{\text{residual}}$ , giving a result of  $-4 \times 10^{-21}$  with a statistical uncertainty of  $3 \times 10^{-20}$  (based on the long-term overlapping ADEV at 10,000 s with the  $\Lambda$ -data [31–33]).

#### 4 LTW scheme with no remote length mismatch using a partial Faraday mirror

In this section, we implement a scheme that automatically suppresses the length mismatch at the remote site. The experimental setup that was used for the work in this section is shown in Fig. 4. We inserted a partial Faraday mirror (p-FM) at the remote setup, which enabled perfect matching of the fiber length in the remote interferometer. When the setup shown in Fig. 4 is compared with that shown in Fig. 1, the action of the p-FM is equivalent to overlapping of the two remote Faraday mirrors in Fig. 1. Thus,  $\delta L_{\text{remote}}$  is zero in this case, and the phase evolution is expected to be given by the two remaining phase error sources,  $\phi_{\text{drift}}$  and  $\phi_{\text{local}}$ .

In Fig. 5a, the measured phase evolution of  $\phi_{\text{LTW}}^{\text{local}} - \phi_{\text{LM}}$  (shown as a thick black line), the estimated phase error due to  $\phi_{\text{drift}}$  (shown as an orange line), the estimated phase error due to  $\phi_{\text{local}}$  (shown as a green line), and the sum of the contributions from the two major phase error sources (shown as a thick pink line) are presented. The phase evolution of  $\phi_{\text{LTW}}^{\text{local}} - \phi_{\text{LM}}$  is again nicely explained as being the sum of the two major phase error sources, and it is free from remote temperature fluctuation in this case.

The fractional frequency instabilities of  $\phi_{\text{LTW}}^{\text{local}} - \phi_{\text{LM}}$  and the two major phase error sources are shown in Fig. 5b, c, respectively. The ADEV and the MDEV that

were calculated from the  $\Pi$ -type counter data started from  $5 \times 10^{-16}$  at 1 s and decreased with slopes of  $-1$  and  $-3/2$ , respectively, which is again as expected for white phase noise. The MDEV that was calculated from the  $\Lambda$ -type counter data started from  $7 \times 10^{-17}$  at 1 s and was limited by the contribution of  $\phi_{\text{drift}}$  after 2000 s, resulting in a minimum instability of  $6 \times 10^{-20}$  at 2000 s. The expected instability of  $\phi_{\text{residual}}$  indicates that the ultimate instability would be  $9 \times 10^{-21}$  at 5000 s if the phase errors due to  $\phi_{\text{drift}}$  and  $\phi_{\text{local}}$  were suppressed. The ultimate accuracy of the frequency comparison with experimental optimization was then estimated by calculating the mean value of the  $\Lambda$ -type frequency data of  $\phi_{\text{residual}}$ , giving a result of  $6 \times 10^{-21}$  with a statistical uncertainty of  $2 \times 10^{-20}$  (based on the long-term overlapping ADEV at 10,000 s with  $\Lambda$ -data [31–33]).

Next, the same laser was used at both sites with no fiber-length mismatch at the remote interferometer to investigate the performance limits of the LTW method. Both  $\phi_{\text{drift}}$  and  $\phi_{\text{remote}}$  were therefore zero in this case.

The measured phase evolution of  $\phi_{\text{LTW}}^{\text{local}} - \phi_{\text{LM}}$  (shown as a thick black line) and the estimated phase error due to  $\phi_{\text{local}}$  (shown as a green line) are shown in Fig. 5d. The result was free from the remote temperature fluctuation as indicated by the temperature data shown in Fig. 5f. The phase evolution that was caused by  $\phi_{\text{local}}$  was less than 0.2 rad because the temperature variation of the local interferometer was relatively small. The phase evolution of  $\phi_{\text{LTW}}^{\text{local}} - \phi_{\text{LM}}$  cannot be explained by  $\phi_{\text{local}}$ , as shown in Fig. 5e, because  $\phi_{\text{local}}$  is one order of magnitude below. This indicates that there are other small unknown residual phase error sources at this instability level of  $1 \times 10^{-20}$ . This corresponds to a phase fluctuation signature that is also present in the error signal (Fig. 5d). This could be attributed to limited rejection of the

**Fig. 4** Experimental setup with no fiber-length-mismatch at the remote site. *p-FM* partial Faraday mirror, *PD* photodiode, *OC* optical coupler, *AOM* acousto-optic modulator, *PLL* phase-locked loop, *b-EDFA* bi-directional erbium-doped fiber amplifier, *PC* polarization controller. The upper part shows the ANC setup on fiber-1, and the lower part shows the LTW setup on fiber-2

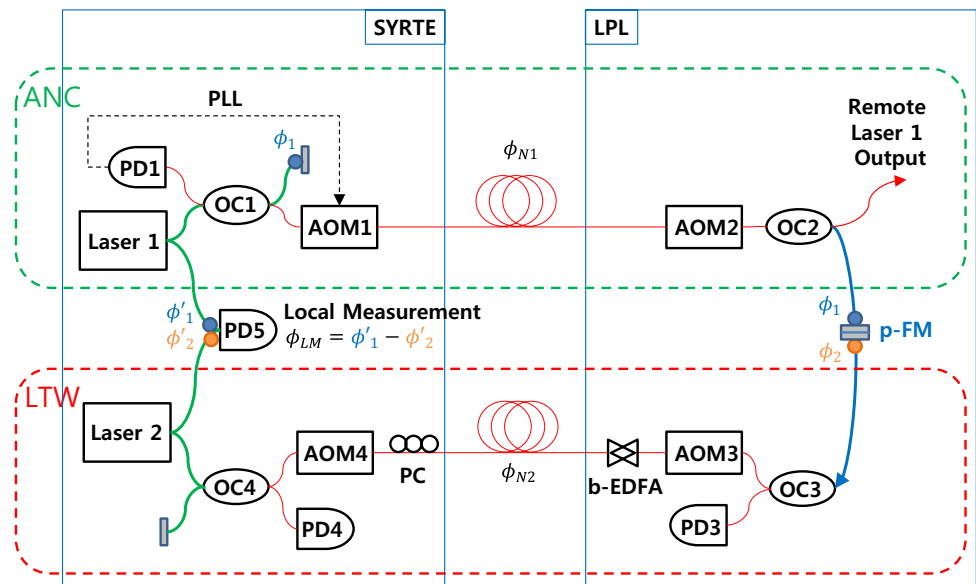
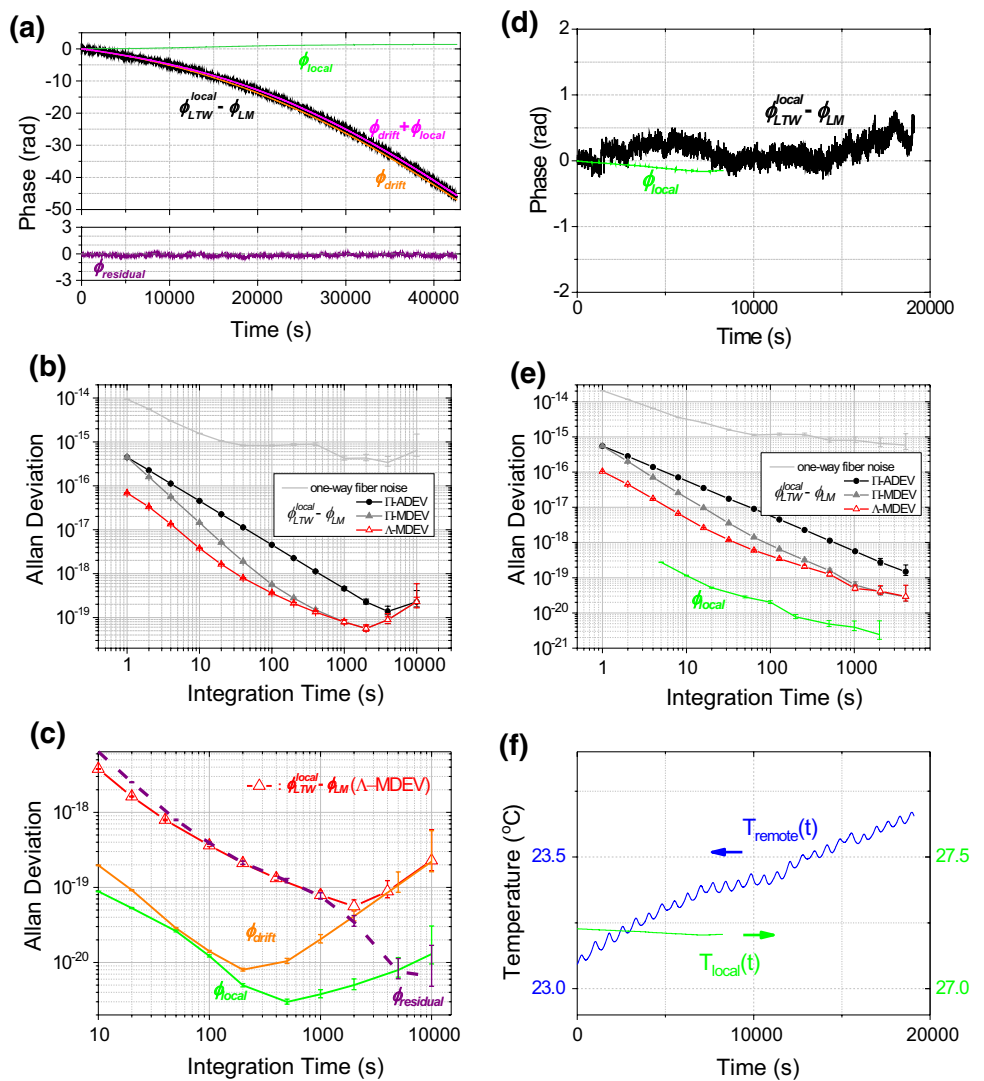


**Fig. 5** **a** Phase evolutions of the local two-way comparison and of the two major phase error sources when there is no fiber-length-mismatch at the remote site ( $\phi_{\text{remote}} = 0$ ).  $\phi_{\text{LTW}}^{\text{local}} - \phi_{\text{LM}}$  is the phase difference between the local two-way measurement and the real local measurement,  $\phi_{\text{drift}}$  is the phase evolution due to the drift of the frequency difference,  $\phi_{\text{local}}$  is the phase evolution caused by the length mismatch in the local interferometer, and  $\phi_{\text{residual}} = \phi_{\text{LTW}}^{\text{local}} - \phi_{\text{LM}} - \phi_{\text{drift}} - \phi_{\text{local}} - \phi_{\text{remote}}$ . **b** Fractional frequency instability of  $\phi_{\text{LTW}}^{\text{local}} - \phi_{\text{LM}}$  in terms of the Allan deviation, **c** the MDEVs of the two major phase error sources. Independent lasers were used at both sites in case of **a–c**. **d** and **e** correspond to the cases of **a** and **b**, respectively, in the case in which the same laser was used at both sites and  $\phi_{\text{remote}} = 0$ . **f** Temperature data of the local interferometer and the remote interferometer in the case of **d** and **e**



laser drift or the fiber noise that is possibly caused by non-reciprocal fiber noise, e.g., as a result of power or polarization effects, which is not cancelled by the ANC method or the two-way setup, or by the instabilities of the electronic detection setup. Further investigation is required to determine the physical effects that are at work at this very low level of instability.

The fractional frequency instabilities of both  $\phi_{\text{LTW}}^{\text{local}} - \phi_{\text{LM}}$  and the estimated phase error due to  $\phi_{\text{local}}$  are shown in Fig. 5e. The ADEV and the MDEV that were calculated from the  $\Pi$ -type counter data started from  $6 \times 10^{-16}$  at 1 s and decreased with slopes of  $-1$  and  $-3/2$ , respectively, which is as expected for white phase noise. The MDEV that was calculated from the  $\Lambda$ -type counter data started from  $1 \times 10^{-16}$  at 1 s, resulting in a minimum instability of  $3 \times 10^{-20}$  at 4000 s. Although the local temperature measurement had actually stopped at 8200 s, it can be seen that there was no bump due to the room temperature effects on the length mismatch at the remote site

in Fig. 5e, as compared to that shown in Fig. 3e, f. The tiny bump around 500 s in Fig. 5e results from the residual phase fluctuations that were discussed above. It is expected that an instability level of  $1 \times 10^{-20}$  would be possible with a longer integration time. The accuracy of the frequency comparison was estimated by calculating the mean value of the  $\Lambda$ -type frequency data of  $\phi_{\text{LTW}}^{\text{local}} - \phi_{\text{LM}}$ , giving a result of  $2 \times 10^{-20}$  with a statistical uncertainty of  $6 \times 10^{-20}$  (based on the long-term overlapping ADEV at 4000 s using the  $\Lambda$ -data [31–33]). It should be noted that this relatively large uncertainty was a result of the short averaging time.

Finally, we introduce one more useful information that can be derived using the hybrid fiber link that has been demonstrated in this article: the expected performance of a uni-directional two-way link [19], in which two separate fibers are used for the uplink and the downlink, can be estimated, with results as shown in Fig. 6. This was obtained by comparing the fiber noise in fiber-1 with the ANC setup with that in fiber-2 with the LTW setup. The results show



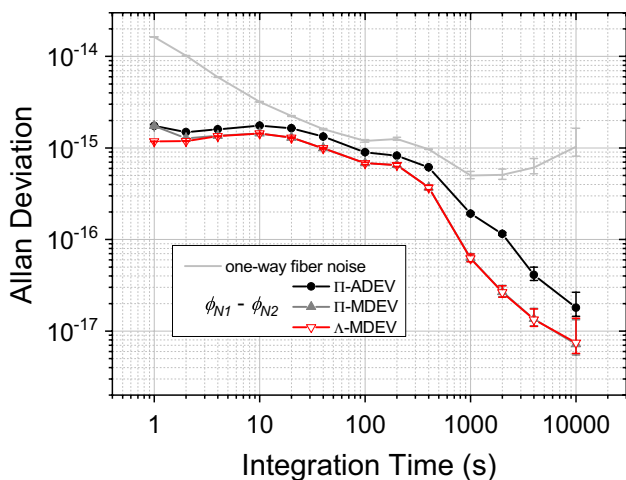


**Fig. 6** Estimate of the expected performance of a uni-directional two-way scheme in terms of the fractional frequency instabilities of the difference of the fiber noise of each fiber with the  $\Pi$ -type counter and the  $\Lambda$ -type counter. ADEV the overlapping Allan deviation, MDEV the modified Allan deviation

that a frequency comparison at a level of  $7 \times 10^{-18}$  at 10,000 s would be possible when using uni-directional two-way measurements. The accuracy of the frequency comparison was estimated using the  $\Lambda$ -type frequency data, and was found to be  $1.0 \times 10^{-17}$  with a statistical uncertainty of  $1.8 \times 10^{-17}$ . This result agrees well with the experimental data reported in [19]. Interestingly, it shows that atomic

fountains can be compared in real time with such a link configuration at mid-range. This offers a convenient option when bi-directional propagation is not available, or when a trade-off must be made between performance and cost.

### 5 Conclusions

We have presented experimental results for a local two-way optical frequency comparison over a 43-km-long urban fiber network using two independent lasers at each of the local and remote sites. The local two-way method does not require synchronization between the remote and local instruments because all required data are obtained locally. Even real-time processing may be possible by using RF devices such as tracking oscillators and frequency mixers for the operations of summation and division that are required to obtain the local two-way result of Eq. 1. Three limiting factors for the LTW comparison scheme (comprising the drift of the frequency difference between the two lasers, and the length mismatches in both the local interferometer and the remote interferometer) have been investigated, and we showed that a fractional frequency instability level of  $10^{-20}$  at approximately 10,000 s was possible when using the LTW method. It should be noted that this is the first time that the laser instability contribution has been demonstrated experimentally. The suppression of the laser drift will be of importance for future optical clock

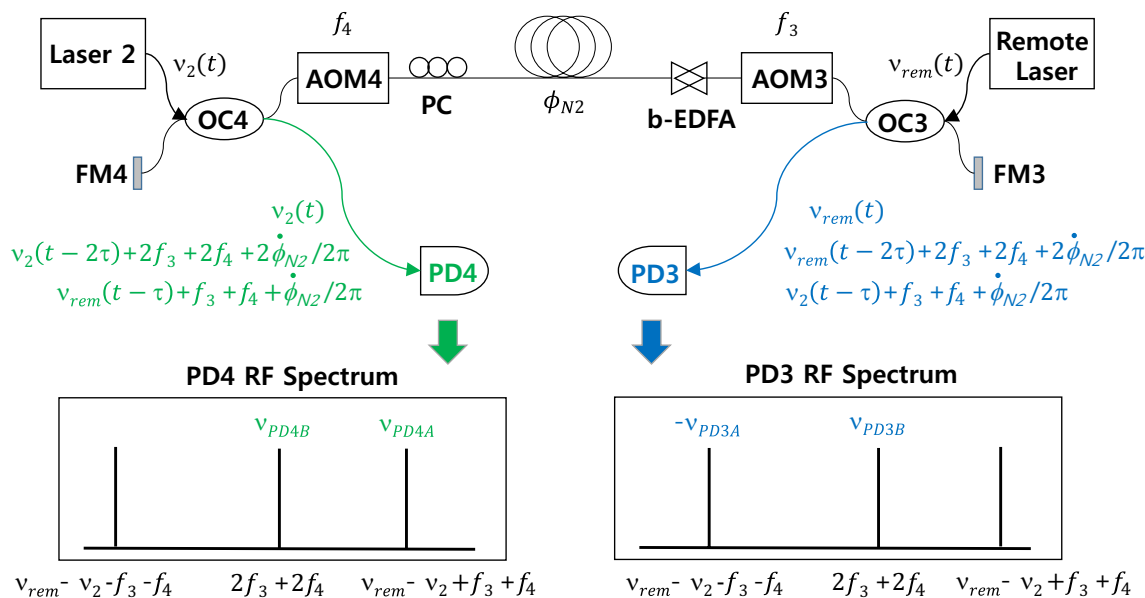


**Fig. 7** Experimental setup and RF signals for the local two-way scheme. PD photodiode, FM Faraday mirror, OC optical coupler, AOM acousto-optic modulator, b-EDFA bi-directional erbium-doped

fiber amplifier, PC polarization controller. Three optical signals that enter each photodiode and the RF spectra are shown

comparisons with longer propagation delay. We also introduced a simple LTW scheme with no length mismatch at the remote site using a partial Faraday mirror. We have showed that the proposed hybrid scheme can provide very useful information on the fundamental limits of optical fiber links, and therefore enhance the transfer capabilities and the self-diagnosis abilities.

### Compliance with ethical standards

**Funding** This work was partly funded from the EC's Seventh Framework Programme (FP7 2007–2013) under Grant Agreement No. 605243 (GN3plus), Action spécifique GRAM, and from the European Metrological Research Programme EMRP under SIB-02 NEAT-FT. The EMRP is jointly funded by the EMRP participating countries within EURAMET and the European Union. W.-K. Lee was supported partly by the Korea Research Institute of Standards and Science under the project "Research on Time and Space Measurements", Grant No. 16011007, and was also partly supported by the R&D Convergence Program of NST (National Research Council of Science and Technology) of Republic of Korea (Grant No. CAP-15-08-KRISS).

**Open Access** This article is distributed under the terms of the Creative Commons Attribution 4.0 International License (<http://creativecommons.org/licenses/by/4.0/>), which permits unrestricted use, distribution, and reproduction in any medium, provided you give appropriate credit to the original author(s) and the source, provide a link to the Creative Commons license, and indicate if changes were made.

### Appendix

We first show that the remote frequency is equal to the local laser frequency at the same time, with no delay, because of the ANC scheme. For simplicity, we suppose that the fiber noise is negligible. Assume that  $\nu_{\text{rem}}(t)$  and  $\nu_{L1}(t)$  are the frequencies of the remote laser and the local laser, respectively, at the entrance of their respective interferometers at time  $t$ .  $\tau$  is the light propagation delay between the local site and the remote site. In that case, the phase at the remote end of fiber-1 is  $\phi_{\text{remote}}(t) = \phi_{L1}(t - \tau) + \phi_C(t - \tau)$ , where  $\phi_C(t - \tau)$  is the correction that is applied at link input end. For ergodic and stationary processes, this correction is given by  $\phi_{L1}(t) - (\phi_{L1}(t - 2\tau) + \phi_C(t - 2\tau) + \phi_C(t)) = 0$ . In a first order approximation, we have  $\phi_C(t - 2\tau) + \phi_C(t) = 2\phi_C(t - \tau)$ . This gives the results that  $\phi_{\text{remote}}(t) = \phi_{L1}(t - \tau) - (1/2)(\phi_{L1}(t - 2\tau) - \phi_{L1}(t)) = \phi_{L1}(t)$  for the first order. Therefore, we have  $\nu_{\text{rem}}(t - \tau) = \nu_1(t - \tau)$ ; in the first order approximation, the laser drift is corrected by the PLL.

Next, we explain the optical signals that enter the photodiodes and the RF output spectra of the photodiodes in the LTW setup. The experimental setup for the LTW scheme only is shown in Fig. 7. Assume that the frequencies of

AOM3 and AOM4 in Fig. 7 are  $f_3$  and  $f_4$ , respectively. The photodiode PD4 receives three main optical signals. One of them is from the remote laser and two of them from the local laser, either directly from the laser source or after a round-trip to the remote site (with reflection on FM3). Their frequencies are given by  $\nu_{\text{rem}}(t - \tau) + f_3 + f_4 + \dot{\phi}_{N2}/2\pi$ ,  $\nu_2(t)$ , and  $\nu_2(t - 2\tau) + 2f_3 + 2f_4 + 2\dot{\phi}_{N2}/2\pi$ , respectively, where  $\dot{\phi}_{N2}$  is the derivative of the fiber phase noise. The two LTW signals on PD4 are the fiber noise-uncompensated phase difference between the two lasers, which is the standard two-way signal, and the round-trip fiber noise. The frequency of the first signal is given by  $\nu_{PD4A} = -\nu_2(t) + [\nu_{\text{rem}}(t - \tau) + f_3 + f_4 + \dot{\phi}_{N2}/2\pi]$ , while that of the second signal is given by  $\nu_{PD4B} = -\nu_2(t) + [\nu_2(t - 2\tau) + 2f_3 + 2f_4 + 2\dot{\phi}_{N2}/2\pi]$ .

Finally, we derive Eq. (4), which describes the phase error in the LTW experiment due to the drift of the frequency difference between the two lasers. An approximate expression for the LTW signal frequency can be given based on the Taylor expansion  $\nu(t - a\tau) = \nu(t) - a\tau \frac{d\nu(t)}{dt} + \frac{(a\tau)^2}{2} \frac{d^2\nu(t)}{dt^2} + O(\tau^3)$ .

$$\begin{aligned} \nu_{PD4A} - \nu_{PD4B}/2 &= -\frac{1}{2}\nu_2(t) + \nu_1(t - \tau) - \frac{1}{2}\nu_2(t - 2\tau) \\ &\approx -[\nu_2(t) - \nu_1(t)] + \tau \left[ \frac{d\nu_2(t)}{dt} - \frac{d\nu_1(t)}{dt} \right] \\ &\quad - \tau^2 \left[ \frac{d^2\nu_2(t)}{dt^2} - \frac{1}{2} \frac{d^2\nu_1(t)}{dt^2} \right] \end{aligned} \quad (8)$$

Because  $\frac{d\nu(t)}{dt}$  and  $\frac{d^2\nu(t)}{dt^2}$  are in the order of 1 Hz/s and 1 Hz/s<sup>2</sup>, and  $\tau$  is approximately  $2 \times 10^{-4}$  s for the 43-km-long fiber link, the third term in Eq. (8) can be neglected. The first term is cancelled when  $\phi_{\text{LTW}}^{\text{local}}$  is compared with  $\phi_{\text{LM}}$ . Therefore,  $\phi_{\text{drift}} = 2\pi \int \tau \left[ \frac{d\nu_2(t)}{dt} - \frac{d\nu_1(t)}{dt} \right] dt = 2\pi \tau [(\nu_2(t) - \nu_1(t)) - (\nu_2(t_0) - \nu_1(t_0))]$ .

### References

1. L.-S. Ma, P. Jungner, J. Ye, J.L. Hall, Delivering the same optical frequency at two places: accurate cancellation of phase noise introduced by an optical fiber or other time-varying path. *Opt. Lett.* **19**(21), 1177–1179 (1994)
2. S.M. Foreman, A.D. Ludlow, M.H.G. de Miranda, J.E. Stalnaker, S.A. Diddams, J. Ye, Coherent optical phase transfer over a 32-km fiber with 1 s instability at  $10^{-17}$ . *Phys. Rev. Lett.* **99**(15), 153601 (2007)
3. H. Jiang, F. Kéfélian, S. Crane, O. Lopez, M. Lours, J. Millo, D. Holleville, P. Lemonde, Ch. Chardonnet, A. Amy-Klein, G. Santarelli, Long-distance frequency transfer over an urban fiber link using optical phase stabilization. *J. Opt. Soc. Am. B* **25**(12), 2029–2035 (2008)
4. G. Grosche, O. Terra, K. Predehl, R. Holzwarth, B. Lipphardt, F. Vogt, U. Sterr, H. Schnatz, Optical frequency transfer via 146 km

- fiber link with  $10^{-19}$  relative accuracy. *Opt. Lett.* **34**(15), 2270–2272 (2009)
5. M. Fujieda, M. Kumagai, S. Nagano, A. Yamaguch, H. Hachisu, T. Ido, All-optical link for direct comparison of distant optical clocks. *Opt. Express* **19**(17), 16498–16507 (2011)
  6. C. Lisdar, G. Grosche, N. Quintin, C. Shi, S.M.F. Raupach, C. Grebing, D. Nicolodi, F. Stefani, A. Al-Masoudi, S. Dörscher, S. Häfner, J.-L. Robyr, N. Chiodo, S. Bilicki, E. Bookjans, A. Koczwar, S. Koke, A. Kuhl, F. Wiotte, F. Meynadier, E. Camisard, M. Abgrall, M. Lours, T. Legero, H. Schnatz, U. Sterr, H. Denker, C. Chardonnet, Y. Le Coq, G. Santarelli, A. Amy-Klein, R. Le Targat, J. Lodewyck, O. Lopez, P.-E. Pottie, A clock network for geodesy and fundamental science. *Nat. Commun.* **7**, 12443 (2016)
  7. K. Predehl, G. Grosche, S.M.F. Raupach, S. Droste, O. Terra, J. Alnis, Th Legero, T.W. Hänsch, Th Udem, R. Holzwarth, H. Schnatz, A 920-km optical fiber link for frequency metrology at the 19th decimal place. *Science* **336**(6080), 441–444 (2012)
  8. O. Lopez, A. Haboucha, B. Chanteau, Ch. Chardonnet, A. Amy-Klein, G. Santarelli, Ultra-stable long distance optical frequency distribution using the Internet fiber network. *Opt. Express* **20**(21), 23518–23526 (2012)
  9. D. Calonico, E.K. Bertaccho, C.E. Calosso, C. Clivati, G.A. Costanzo, M. Frittelli, A. Godone, A. Mura, N. Poli, D.V. Sutyryn, G. Tino, M.E. Zucco, F. Levi, High-accuracy coherent optical frequency transfer over a doubled 642-km fiber link. *App. Phys. B* **117**(3), 979–986 (2014)
  10. T. Rosenband, D.B. Hume, P.O. Schmidt, C.W. Chou, A. Brusch, L. Lorini, W.H. Oskay, R.E. Drullinger, T.M. Fortier, J.E. Stalnaker, S.A. Diddams, W.C. Swann, N.R. Newbury, W.M. Itano, D.J. Wineland, J.C. Bergquist, Frequency ratio of  $\text{Al}^+$  and  $\text{Hg}^+$  single-ion optical clocks; metrology at the 17th decimal place. *Science* **319**(5871), 1808–1812 (2012)
  11. W. Yang, D. Li, S. Zhang, J. Zhao, Hunting for dark matter with ultrastable fibre as frequency delay system. *Sci. Rep.* **5**, 11469 (2015)
  12. P.A. Williams, W.C. Swann, N.R. Newbury, High-stability transfer of an optical frequency over long fiber-optic links. *J. Opt. Soc. Am. B* **25**(8), 1284–1293 (2008)
  13. A. Matveev, C.G. Parthey, K. Predehl, J. Alnis, A. Beyer, R. Holzwarth, Th Udem, T. Wilken, N. Kolachevsky, M. Abgrall, D. Rovera, Ch. Salomon, P. Laurent, G. Grosche, O. Terra, Th Legero, H. Schnatz, S. Weyers, B. Altschul, T.W. Hänsch, Precision measurement of the hydrogen  $1\text{S}$ – $2\text{S}$  frequency via a 920-km fiber link. *Phys. Rev. Lett.* **110**(23), 230801 (2013)
  14. B. Argence, B. Chanteau, O. Lopez, D. Nicolodi, M. Abgrall, Ch. Chardonnet, C. Daussy, B. Darquié, Y. Le Coq, A. Amy-Klein, Quantum cascade laser frequency stabilization at the sub-Hz level. *Nat. Photon.* **9**(7), 456–461 (2014)
  15. C. Clivati, G. Cappellini, L. Livi, F. Poggiali, M. Siciliani de Cumis, M. Mancini, G. Pagano, M. Frittelli, A. Mura, G.A. Costanzo, F. Levi, D. Calonico, L. Fallani, J. Catani, M. Inguscio, Measuring absolute frequencies beyond the GPS limit via long-haul optical frequency dissemination. *Opt. Express* **24**(11), 11865–11875 (2016)
  16. C. Clivati, G.A. Costanzo, M. Frittelli, F. Levi, A. Mura, M. Zucco, R. Ambrosini, C. Bortolotti, F. Perini, M. Roma, D. Calonico, A coherent fiber link for very long baseline interferometry. *IEEE T. Ultrason. Ferr.* **62**(11), 1907–1912 (2015)
  17. C. Ma, L. Wu, Y. Jiang, H. Yu, Z. Bi, L. Ma, Coherence transfer of subhertz-linewidth laser light via an 82-km fiber link. *Appl. Phys. Lett.* **107**(26), 261109 (2015)
  18. C.E. Calosso, E. Bertacco, D. Calonico, C. Clivati, G.A. Costanzo, M. Frittelli, F. Levi, A. Mura, A. Godone, Frequency transfer via a two-way optical phase comparison on a multiplexed fiber network. *Opt. Lett.* **39**(5), 1177–1180 (2014)
  19. A. Bercy, F. Stefani, O. Lopez, Ch. Chardonnet, P.-E. Pottie, A. Amy-Klein, Two-way optical frequency comparisons at  $5 \times 10^{-21}$  relative stability over 100-km telecommunication network fibers. *Phys. Rev. A* **90**(6), 061802(R) (2014)
  20. F. Stefani, O. Lopez, A. Bercy, W.-K. Lee, Ch. Chardonnet, G. Santarelli, P.-E. Pottie, A. Amy-Klein, Tackling the limits of optical fiber links. *J. Opt. Soc. Am. B* **32**(5), 787–797 (2015)
  21. D.W. Hanson, Fundamentals of two-way time transfer by satellite, in *Proceedings of 43rd Annual Frequency Control Symposium*, (IEEE, Denver, CO, Piscataway, NJ, 1989), pp. 174–178. doi:10.1109/FREQ.1989.68861
  22. F.R. Giorgetta, W.C. Swann, L.C. Sinclair, E. Baumann, I. Codrington, N.R. Newbury, Optical two-way time and frequency transfer over free space. *Nat. Photon.* **7**(6), 434–438 (2013)
  23. ICOF (International Clock Comparisons via Optical Fiber), <http://geant3plus.archive.geant.net/opencall/Optical/Pages/ICOF.aspx>. Accessed 27 Apr 2017
  24. J. Kronjäger, G. Marra, O. Lopez, N. Quintin, A. Amy-Klein, W.-K. Lee, P.-E. Pottie, H. Schnatz, Towards an international optical clock comparison between NPL and SYRTE using an optical fiber network. Presented at the 30th European Frequency and Time Forum, York, United Kingdom (2016). <http://www.eftf2016.org/>. Accessed 29 April 2017
  25. W.-K. Lee, F. Stefani, A. Bercy, O. Lopez, A. Amy-Klein, P.-E. Pottie, Strengthening capability of optical fiber link with hybrid solutions, 8th Symposium on Frequency Standards and Metrology 2015, Poster E05, p 155, Potsdam, Germany (2015). <https://www.ptb.de/8fsm2015/>. Accessed 29 April 2017
  26. F. Kéfélian, O. Lopez, H. Jiang, Ch. Chardonnet, A. Amy-Klein, G. Santarelli, High-resolution optical frequency dissemination on a telecommunications network with data traffic. *Opt. Lett.* **34**(10), 1573–1575 (2009)
  27. H. Jiang, “Development of ultra-stable laser sources and long-distance optical link via telecommunication networks,” Ph. D. thesis (2010), <https://tel.archives-ouvertes.fr/tel-00537971>. Accessed 27 Apr 2017
  28. G. Kramer, W. Klische, Multi-channel synchronous digital phase recorder. in *Proceedings of the 2001 IEEE International Frequency Control Symposium and PDA Exhibition*, pp. 144–151 (2001). doi:10.1109/FREQ.2001.956178
  29. S. Dawkins, J. McFerran, A. Luiten, Considerations on the measurement of the stability of oscillators with frequency counters. *IEEE Trans. Ultrason. Ferroelectr. Freq. Control* **54**(5), 918–925 (2007)
  30. E. Rubiola, On the measurement of frequency and of its sample variance with high-resolution counters. *Rev. Sci. Instrum.* **76**(5), 054703 (2005)
  31. N. Chiodo, N. Quintin, F. Stefani, F. Wiotte, E. Camisard, C. Chardonnet, G. Santarelli, A. Amy-Klein, P.-E. Pottie, O. Lopez, Cascaded optical fiber link using the internet network for remote clocks comparison. *Opt. Express* **23**(26), 33927–33937 (2015)
  32. A. Bercy, O. Lopez, P.-E. Pottie, A. Amy-Klein, Ultrastable optical frequency dissemination on a multi-access fibre network. *Appl. Phys. B* **122**, 189 (2016)
  33. S.M.F. Raupach, A. Koczwar, G. Grosche, Brillouin amplification supports  $1 \times 10^{-20}$  uncertainty in optical frequency transfer over 1400 km of underground fiber. *Phys. Rev. A* **92**(2), 021801(R) (2015)
  34. W.-K. Lee, D.-H. Yu, C.Y. Park, J. Mun, The uncertainty associated with the weighted mean frequency of a phase-stabilized signal with white phase noise. *Metrologia* **47**(1), 24 (2010)